Defence Science Journal, Vol. 59, No. 1, January 2009, pp. 63-72
© 2009, DESIDOC

Ray-Trace of an Abnormal Radar Echo Using Geographic Information System

Chi-Nan Chen[1,2], Jian-Liang Wang[2], Chang-Min Chu[3], and Fang-Chuan Lu[3]

[1]*Military Acacemy, Republic of China*
[2]*Chung Cheng Institute of Technology, National Defense University, Republic of China*
[3]*Nan Jeon Institute of Technology, Republic of China*

ABSTRACT

Weather radar plays a key role in natural disaster mitigation just as surveillance radar does in detecting objects that threaten homeland security. Both together comprise an instrumental part of radar observation. Therefore, quality control of the data gathered through radar detection is extremely important. However, radar waves propagate in the atmosphere, and an anomalous echo can occur if there are significant discontinuities in temperature and humidity in the lower boundary layer. The refractive curvature of the earth makes some errors in observation inevitable. On the night of July 3, 2003, Next Generation Radar (NEXRAD) weather radar detected an abnormal echo. The Weather Research and Forecast (WRF) model was utilized to simulate the atmospheric conditions. Radar propagation was simulated using the Advanced Refractivity Engineering Prediction System (AREPS) as well as the GIS. The results show the feasibility of establishing an abnormal propagation early-warning system and extending the application of the GIS in serving as the foundation of a Common Operation Picture (COP). Furthermore, the parameters of the boundary layer near the sea's surface in the numerical weather forecasting model need remodification.

Keywords: Atmospheric refractivity, geographic information system (GIS), weather research and forecast model (WRF), common operational picture (COP)

1. INTRODUCTION

Taiwan, which is located in the northwestern Asian Pacific Rim, has towering mountain ranges running from north to south and diverse weather features. The weather systems that cause most of Taiwan's precipitation during the rainy season are fronts, typhoons and afternoon convections. These systems, which frequently cause natural disasters, cause meteorological problems for both meteorologists and the public (Kuo and Chen[1]; Lin[2]; Chen and Chou[3]).

Taiwan's Central Weather Bureau (CWB) recently started using instant reflectivity observed by weather radar to improve precipitation forecasting in the Quantitative Precipitation Estimation-Segregation Using Multiple Sensors (QPE-SUMS) and other related early-warning systems (Chen *et al.*[4]). In order to monitor and predict water-related hazards, a system called "very short-term quantitative precipitation forecasts" (VSTQPF) (Vasiloff *et al.*[5]) is under development by the National Severe Storms Laboratory in the United States. Therefore, accurate weather radar observation is extremely important in short-term weather forecasting.

While quantitative precipitation estimates using radar are well developed, failure to recognize the effects of anomalous propagation may lead to forecasting errors (Moszkowicz *et al.*[6]). Borsum[7] describes a case in which anomalous propagation conditions resulted in a Doppler radar echo from a 2400 m high mountain that was attributed to nonexistent thunderclouds supposedly towering up to 11,000 m and containing velocities as high as 18 m s^{-1}. This echo persisted at radar elevation angles of up to 3.5°.

Lu *et al.*[8] found during an evaporation duct experiment overseas off southeastern Taiwan that the duct can be as high as 120 m above the sea surface when intensive Pacific high-pressure is controlling the weather. In such cases, the sky is clear and wind velocity is low. This evaporation duct extends the search range of ships and anti-submarine radar, as the effective range of electronic devices extends to 350 km.

With increased computer computational speeds and storage, the numerical weather model has gradually become the primary tool for meteorological research. Atkinson, *et al.*[10] utilised a numerical model to simulate the Marine Internal Boundary Layer (MIBL) status in the Persian Gulf, the results of which are helpful in understanding the occurrence and location of ducts. However, their findings require improvements in duct thickness and intensity. Zhu and Atkinson[10] used the Mesoscale Model (MM5) to derive the climatic characteristics of atmospheric refractions in the Persian Gulf, noting that atmospheric refraction is affected by marine terrain, seasons and diurnal alternate. Haack and Burk[10] used the Coupled Ocean-Atmosphere Mesoscale Prediction System (COAMPS) developed by the US Navy to simulate and forecast summertime atmospheric refraction in a marine boundary layer in the California coastal area. The correct forecast probability of surface duct was

Received 31 March 2008

approximately 82 per cent, while the height of the MIBL was low and duct intensity was weak.

According to the US Unidata planning blueprint of 2008, the GIS will be the operational platform for integrating spatial information in scientific research (Habermann[12], Ramamurthy[13], Shipley[14]). Kucera, *et al*.[15] investigated the effects of terrain interference of radar waves in Guam using the GIS with different terrain resolutions. Krajewaski, *et al*.[16] utilized the GIS to map the relationship between radar wave propagation and terrain at the US's KRLX (Charleston, West Virginia) and KEMX (Tucson, Arizona) radar stations. However, these two studies only used single point vertical profile data less than 1 km in height as the reference atmospheric refractivity and did not include data for a wider area.

Xie, *et al*.[17] developed a GIS scheme for automatic processing of Next Generation Radar (NEXRAD) Level III precipitation data. However, Level II data is processed in this study. The US National Ocean and Atmosphere Administration (NOAA) provides some Java tools to convert NEXRAD Level II data (NOAA NCDC website). Unfortunately, these java tools encounter projection problems when Wufensan data are inputted. Additionally, other weather radar systems have different data formats in Taiwan. For the convenience of using the meteorological data application in Microsoft Windows, this study integrates radar observations, weather numerical model output and geographic data to simulate ray traces in GIS (ArcView).

Many disciplines are utilising computer science and technology to conduct revolutionary planning and concrete operations, and the military is no exception. Under the joint task framework of C^{4}ISR (Command, Control, Communication, Computer, Intelligence, Surveillance, and Reconnaissance), net-centric processes and mass transit information, a common operational picture (COP) has been created with the purpose of sharing situational battle space awareness. That is an achievement in information sharing. The US Chairman of the Joint Chiefs of Staff instruction guide *"Global Command and Control System Common Operational Picture Reporting Requirements"* (CJCSI 3151.01A) points out that a COP will control battlefield conditions effectively under appropriate management. However, it also emphasizes that adjustments are needed in order to be consistent with forces and tasks.

Keuhlen, *et al*.[18] pointed out that a COP is not only an integrated information system for providing battle space awareness, in accordance with new and growing intelligence, but also for putting the right information in the right hands at the right time to make effective decisions. Richmond, *et al*.[19] point out that land warfare decision-makers are particularly interested in on-ground mobility characteristics of battlefields. The Mobility-COP design team identified 8 key categories: terrain, obstacles, weather, maneuver analysis, route planning, threat analysis, forces, and utilities. Weather consists of current and forecasted weather conditions (e.g., visibility, precipitation, etc.), which affect mobility and maneuverability.

Although earlier methods of radar data analysis for refraction have generally been successful, numerical forecasting can be used for early warning of possible abnormal echo areas and avoiding inaccurate radar observations. More importantly, radar blind zones due to abnormal radar propagation could be better controlled as search and surveillance capability is enhanced. Therefore, ideal numerical forecasting incorporates the Geographic Information System (GIS), an analysis of radar ray trace, and an evaluation of the feasibility of establishing an abnormal propagation early-warning system. This system would assist meteorologists and battlefield commanders to maintain a suitable atmospheric condition.

The primary purpose of the study reported in this paper is to utilise a numerical weather model to recreate the atmospheric condition involving a weather radar abnormal echo case which took place on July 3, 2003 at Wufensan in Taiwan. The US Advanced Refractive Effects Prediction System (AREPS) is adapted to investigate the simulated refractivity. The GIS displays the refractive decision aids and a radar propagation prototype with terrain interference to determine radar waves at the sea's surface. The flow chart of this research is shown in Fig. 1. Section 2 below introduces the atmospheric refraction theory. Section 3 describes the radar anomaly echo case and weather model simulation. Section 4 demonstrates 2-D, one-direction ray trace in AREPS and 3-D ray trace in the GIS to evaluate the feasibility of a radar abnormal echo early warning system. Section 5 comprises a discussion of the results and suggestions for future research.

2. ATMOSPHERIC REFRACTIVITY

Nonstandard refraction (anomalous propagation) of electromagnetic radiation in the lower troposphere may cause radio or radar signals to propagate so that the curvature of their path is greater than the earth's surface curvature. These microwaves may then become trapped within this duct layer and travel beyond the horizon. Propagation of microwave and millimeter-wave electromagnetic radiation in the atmosphere is determined by gradients of the refractive index of air. Because it is very close to unity, this refractive

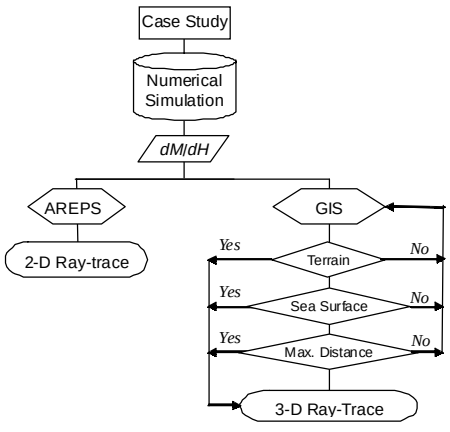

Figure 1. The flowchart of this research.

index n is represented by a scaled quantity called the radio refractivity N. Debye's[20] theory has been used to express refractivity N in terms of atmospheric pressure, water vapor pressure, and temperature (Bean and Dutton[21]). These expressions are given by

$$N = (n-1)\times 10^6 = \frac{77.6}{T}\left(p + \frac{4810e}{T}\right) \quad (1)$$

where T (K) is the atmospheric temperature, p (hPa) is the total atmospheric pressure, and e (hPa) is the water vapor pressure. The constants are empirically derived from dielectric constant measurements and are valid for radio frequencies between 1 and 100 GHz (Babin[22], Babin *et al.*[23]). Currently, most weather radar frequencies are 3–10 GHz (C-Band wavelength, 5 cm; S-Band wavelength, 10 cm) (Rinehart[24]). Modified refractivity M, which takes the earth's curvature into account, is related to radio refractivity N whereby r_e is the earth's radius and z is altitude in meters.

$$M = N + \frac{z}{10^{-6} r_e} \approx N + 0.157z \quad (2)$$

Based on the vertical gradient of modified refractivity (*dMdH*), refractions can be divided into the following four categories: sub-refraction ($dMdH > 157\ M$ km^{-1}), standard refraction ($79 < dMdH = 157\ M$ km^{-1}), super-refraction ($0 < dMdH = 79\ M$ km^{-1}), and trap refraction ($dMdH = 0\ M$ km^{-1}). Figure 2 presents the radio propagation of refractive conditions.

The AREPS provided by the US Navy Space and Naval Warfare Systems Center computes and displays a number of tactical decision aids. These are airborne and surface-based radar capable of determining probability of detection, electronic surveillance measure (ESM) vulnerability, UHF to EHF communications, and a surface-search range table.

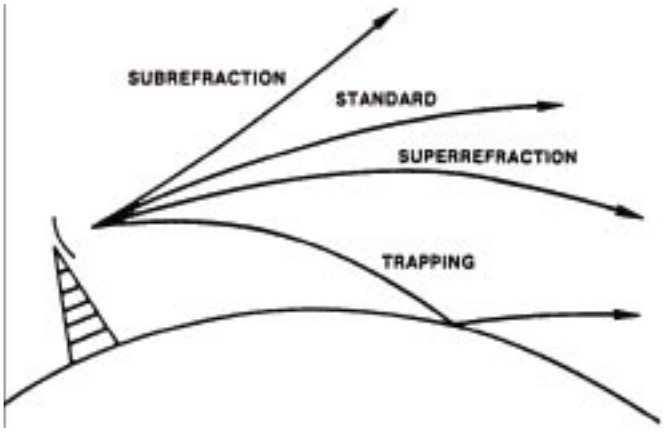

Figure 2. Refractive conditions (adopted from Patterson *et al*[25]).

All decision aids are based on electromagnetic (EM) system parameters stored in a changeable database. Paths containing land features depend on terrain data. All calculations depend on atmospheric refractivity data derived from radiosondes or other sensors. The propagation model used is the Advanced Propagation Model (APM). AREPS creates a height versus range coverage or surface-search range diagram for each azimuth desired (Patterson *et al*[25]).

However, the web edition mainly provides simulation of profile data at a single point, and the ray trace of an electromagnetic wave is affected by the atmospheric condition where the wave propagates. Thus, the atmospheric condition must be considered when simulating real electromagnetic wave traces.

To define ray trace, in which height is a function of distance, Rinehart[24] proposed the following equation:

$$h = \sqrt{r^2 + R'^2 + 2rR'\sin(\theta_e)} - R' + h_0 \quad (3)$$

where h is height (compared with radar height), r is the lean distance of radar waves, R' represents earth's radius and stands for the atmospheric refractive status, θ_e is the elevation angle of the radar beam, and h_0 is the height of the radar antenna (compared with radar height). Since atmospheric refractivity cannot be determined from only a single profile, the atmospheric construction of beam paths must be considered.

The ray trace equations of AREPS are based on small angle approximations to Snell's law and the assumption of a linear variation of modified refractivity, M. Rays reflected from the sea's surface are assumed to have equal incident and reflected angles. At each step within the ray trace, a M-unit gradient is needed. Figure 3 illustrates a range-dependent ray (sloping layers) with a positive launch angle (Patterson *et al*[25]). The vertical gradient is considered and is given as $dMdh_j = 10^{-3}(M_{j+1} - M_j)/(H_{j+1} - H_j)$ where M_j denotes the jth vertical element in the M-unit array, and the H_j denotes the corresponding jth vertical element in the height array. Negative values of $dMdh_j$ are trapping layers. A standard atmosphere (4/3 earth) gradient is defined as the gradient above the highest height array element. That is, $dMdh_{j+1} = 0.000118$, where j is the index of the last element in the H array.

Gabella and Pernoa[26] utilised Fortran to program simulations of terrain effects on radar waves propagated in standard atmosphere according to the digital elevation model (DEM). Due to limited computer capability and the method for acquiring atmospheric profiles, only single vertical profiles

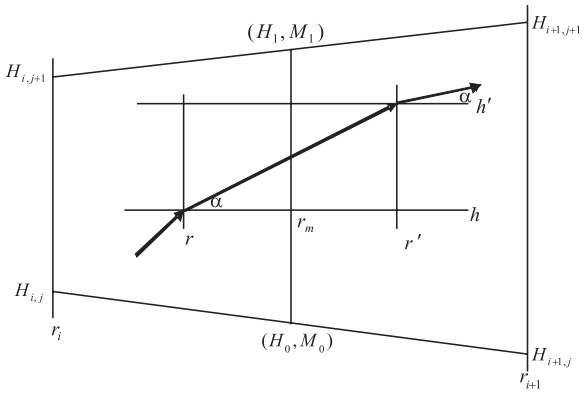

Figure 3. Raytrace variables (adopted from Patterson *et al*[25]).

could be simulated in the past. However, with the development of high speed computers and more advanced GIS-related technology, 3-D ray-trace simulation is now possible.

The need for accurate environmental data is a significant challenge in the field of earth sciences. Scholars have integrated meteorological information with the GIS. Siddiqui *et al*[27] utilized satellite imagery and GIS to assess variations in forests and farmland. Ng, *et al*[28] applied the GIS in analyzing floating particles in New York City after 9/11. Wilhelmi and Brunskill[29] identified the advantages of applying the GIS to meteorological processes. Wilhelmi and Betancourt[30] demonstrated the numerical weather model forecasts and observational data in the GIS and exhibited the results for radar and ground observations in generating a novel presentation for meteorology researchers. Yuan[31] noted that the GIS is not only a mapping software but that it has further applications in weather forecasting, tornado damage analysis and flood analysis.

3. CASE STUDY AND SIMULATIONS

For continual monitoring of precipitation originating from the ocean, Taiwan's Central Weather Bureau (CWB) operates a weather radar observation network with four stations, such as the RCWF station in northern Taiwan (Fig. 4a), that are instrumental in predicting heavy rains. Based on reflectivity observations from the RCWF, the echo appeared over the sea off radar station's southeastern coast and was detected by the radar station at 07 UTC (local time is +8 h) on July 3, 2003. This echo moved from the southeast in a northwesterly direction. The large-scale precipitation echo, which reached 45 dBZ in intensity, appeared over the sea northwest of Taiwan, 100–180 km from the radar station, from 14 UTC on July 3rd to 00 UTC on July 4th. The echo subsequently weakened before disappearing at 06 UTC on July 4th (Fig. 4b only shows the echo at 18 UTC on July 3rd).

During weather radar observation, when a precipitation echo exists and peaks in intensity at 45 dBZ, based on the Z-R relation (Rinehart[24]), estimated from convectional summer precipitation, the rainfall rate could be as high as 28 mm h^{-1}. However, when assessing the cumulative precipitation during that period, no rainfall records exist for northern Taiwan (figures not shown). Based on the infrared satellite image (Fig. 4c), only thin clouds covered the northern part of Taiwan and these clouds moved from north to south, opposite the surface wind, indicating that these clouds were not part of the sustained precipitation echo. During this period, a Pacific high pressure surrounded Taiwan, resulting in a cloud-free night. Chu *et al*[32] provide more detailed analyses about synoptic weather, radar reflectivity, radial wind, and spectrum.

Due to the abnormal echo that took place the night of July 3, 2003, no advanced observational data were available in Taiwan, especially over the ocean. Therefore, a numerical weather model was utilised to reconstruct the atmospheric condition in and around Taiwan. The Weather Research and Forecast (WRF) V2.1.2 developed by the U.S. National Center for Atmospheric Research (NCAR) was adopted (Skamarock *et al*[33]). The WRF is formulated using a terrain-following mass coordinate (η) and only the upper boundary is fixed at 50 hPa during simulation. In order to enhance the vertical resolution of the lower atmosphere, 35 layers have been vertically divided. There are about 17 layers below a ceiling of 1.5 km; the parameter settings are shown in detail in Table 1. The height of the layer closest to the ground is about 4 m while the second layer is about 26 m (staggered grid). The main purpose is to determine variations in atmospheric refractivity in vertical directions near the radar area.

To meet the concept of weather scale, 3 nested domains were designed with horizontal grid lengths of 45, 15 and 5 km. The corresponding area with latitude and longitude

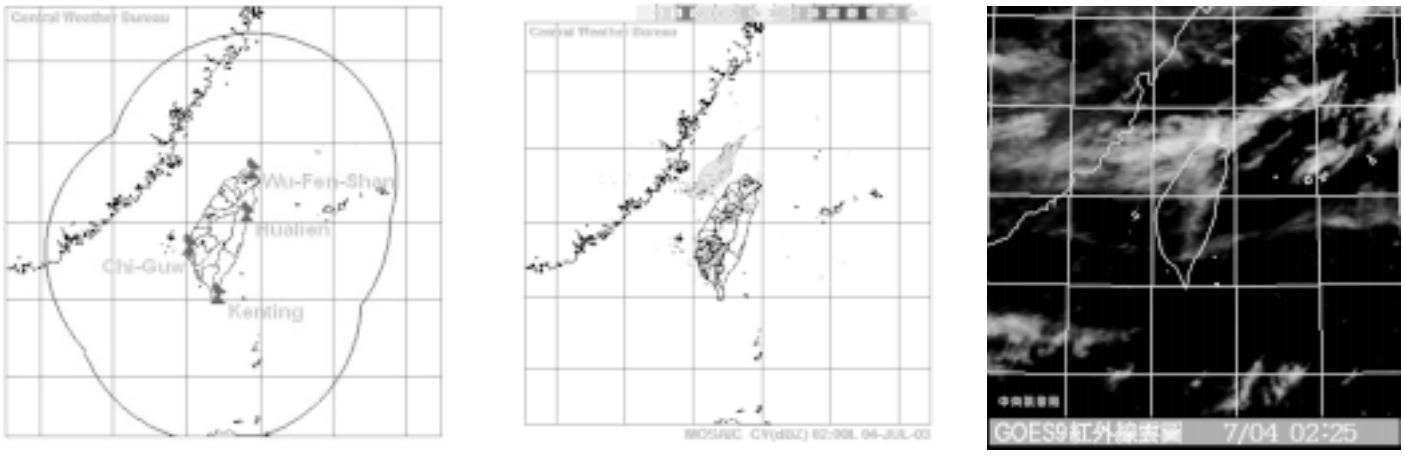

(a) (b) (c)

Figure 4. Radar network of CWB and observation of 18UTC, July 3, 2003, (a) Radar Network in Taiwan, the red line indicates the monitor range, (b) Composite radar scan volume , color indicates reflectivity, the interval is 5 dBZ, shown as the color bar, (c) Infra-red cloud image (data source: CWB).

Table 1. Parameter settings in simulation

Domains	D01	D02	D03
Size in grids	130*110	130*127	180*180
Horizontal grid length	45 km	15 km	5 km
Time step	90 s	30 s	10 s
Integration time	36 h, July 3, 2003 00 UTC~July 4, 2003 12 UTC		
Vertical levels	35 levels, η = 0.999, 0.995, 0.990, 0.979, 0.968, 0.957, 0.946, 0.935, 0.924, 0.913, 0.902, 0.890, 0.878, 0.866, 0.854, 0.842, 0.839, 0.816, 0.791, 0.764, 0.736, 0.707, 0.677, 0.645, 0.612, 0.577, 0.540, 0.500, 0.456, 0.408, 0.354, 0.289, 0.204		
Map projection	Mercator, domains are shown in Fig. 5		
Dynamical core	Eulerian mass		
Hydrostatic/ non-hydrostatic	Hydrostatic		Non-hydrostatic
Cumulus	Kain-Fritsch (new Eta)		Not used
Microphysics	WSM 5-Class scheme		
Boundary layer	YSU scheme		
Long wave radiation	rrtm scheme		
Short wave radiation	Dudhia scheme		
Surface layer	Monin-Obukhov scheme		
Land-surface	Noah scheme		

grid references is shown in Fig. 5. The Monin-Obukhov scheme was adopted for the surface layer while the boundary layer was adopted for the YSU scheme. The WSM-5 microphysics was adopted to include water vapour, cloud, and precipitation processes.The grid length above 15 km adopted the hydrostatic scheme while the Kain-Fritsch (new Eta) cumulus scheme was used to calculate the sub-grid-scale effects of convective and/or shallow clouds.

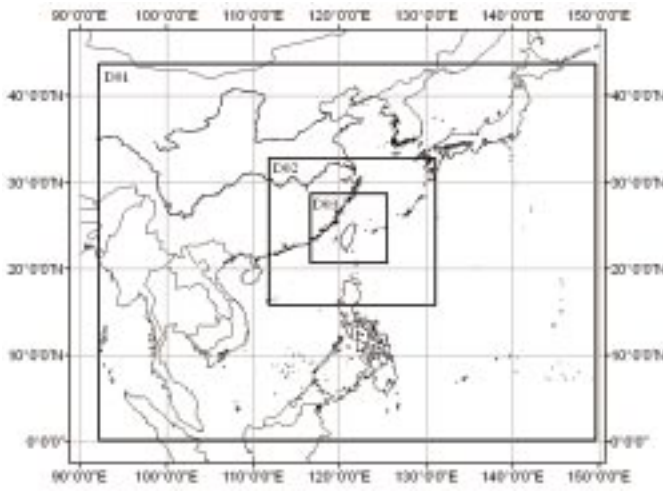

Figure 5. Three nested grids of simulation (in Mercator projection and latitude and longitude grid reference).

Furthermore, the time steps were 90, 30 or 10 s, depending on grid length. Simulation took place from 00UTC on July 3rd 2003 to 12 UTC on July 4th for a total of 36 h. The initial data adopts the U.S. National Center of Environment Prediction (NCEP) Final Analysis, a global analysis with 1°×1° horizontal resolution, 28 layers vertically oriented, and an interval time of 6 h. The initial data also include lateral boundary conditions.

Chu *et al.*[32] demonstrate some simulation results of this study case. Since southwestern currents bring moisture to northern Taiwan, an obvious trapping layer exists around Taiwan. This is the most important factor accounting for why the abnormal echo occurred. The main purpose of this paper is to apply the numerical weather model to radar wave ray trace simulation in an effort to determine the feasibility of establishing an abnormal propagation early warning radar system.

4. SIMULATION OF RADAR RAY TRACE

Figure 6 shows the column vector (CV) at 15 UTC on July 3rd and at 00 UTC on July 4th as well as atmospheric refraction thematic charts. At 15 UTC on July 3rd, a radar echo appeared 100 km northwest of the RCWF, while trapping occurred at the RCWF (Figs. 6a and 6b). However, no apparent duct layer appeared over the northern coast. Thus, we conclude that the electromagnetic wave did not propagate in the theoretical path after being transmitted from the station and reached the sea in a very short time. At 00 UTC on July 4th, trapping layers of different intensities appeared over the sea near Taiwan, especially in the west. However, no trapping occurred at the RCWF. The wave path was high when it reached the sea. The warm wet air resulted in the trapping layer. Thus, the echo location was northwest of the radar station (Figs. 6c and 6d).

The distribution of the trapping layer is in accordance with radar observations and is similar to Persian Gulf simulation results obtained by Atkinson *et al*[9] indicating that a duct always exists over a strait. Figure 6 presents all possible atmospheric refraction for the RCWF and other radar stations. Moreover, the trapping layer over the sea is parallel to the coast due to its geographic location and the warm wet air brought by the southwest jet stream. Thus, the echo is linear and parallel to the terrain. To apply refraction information to potential decision aids, trapping layer positions are displayed as references for radar operators during weather monitoring.

In order to validate numerical simulation of refractivity, AREPS is utilized for duct analysis and radar propagation. Figure 7 shows atmospheric refraction at a point close to Taiwan's northwestern coast. The WRF simulation results demonstrate that super refraction and trapping existed close to the coast at an elevation of <500 m. The thickness of the trapping extended from the ground to 400 m in height. Due to the apparent atmospheric refraction over the sea, radar waves were trapped and bended downward toward the sea.

By using atmospheric profiles and simulating radar

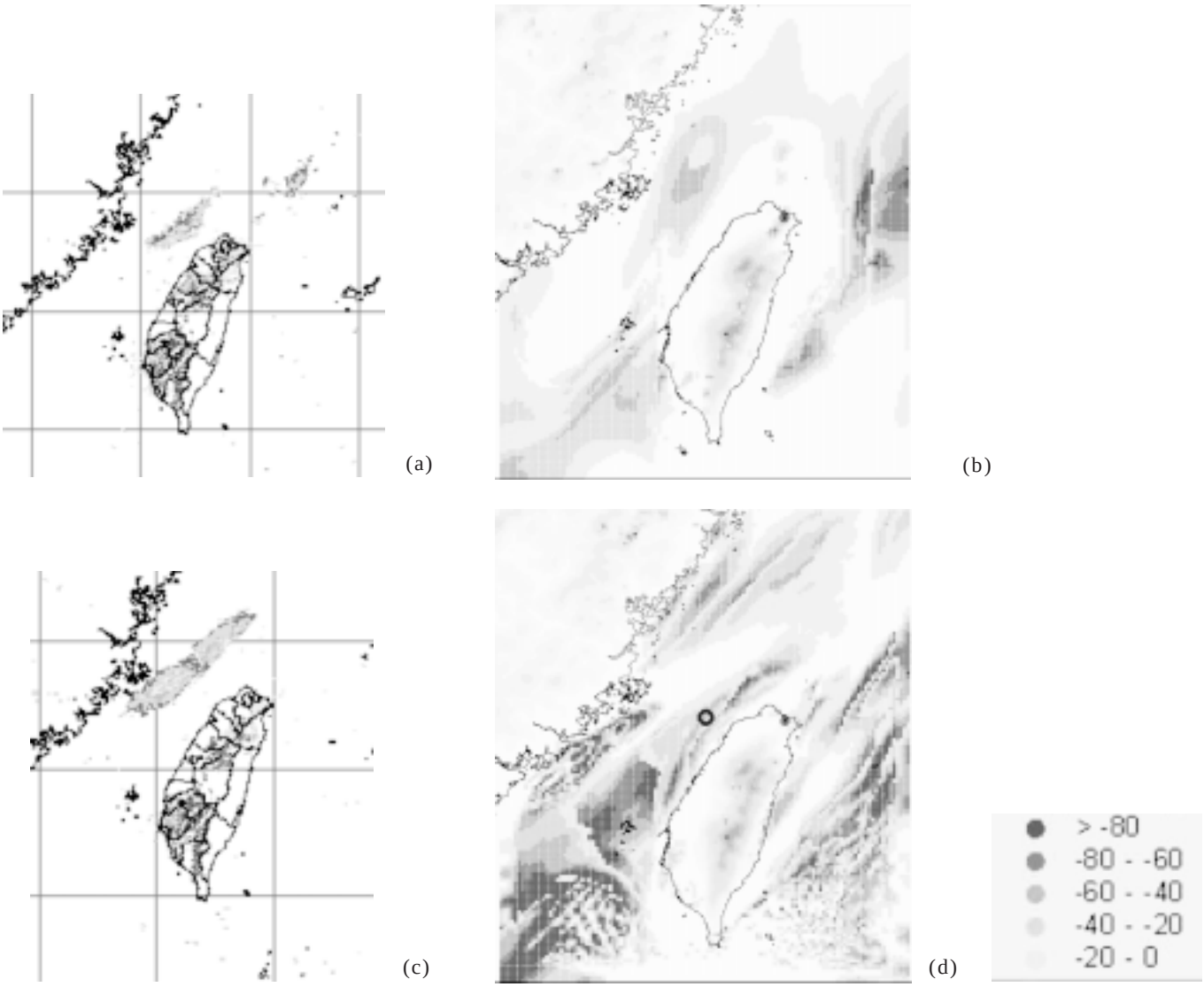

Figure 6. Composite reflectivity and atmospheric refractivity chart, (a) and (b) are July 3, 15 UTC, (c) and (d) are July 4, 00 UTC. The color indices of composite reflectivity are same as in Fig. 4. For the atmospheric refractivity chart, green indicates terrain; color indicates the location and intensity of trapping layer. Blue circle on (d) is the selected point of Fig. 7.

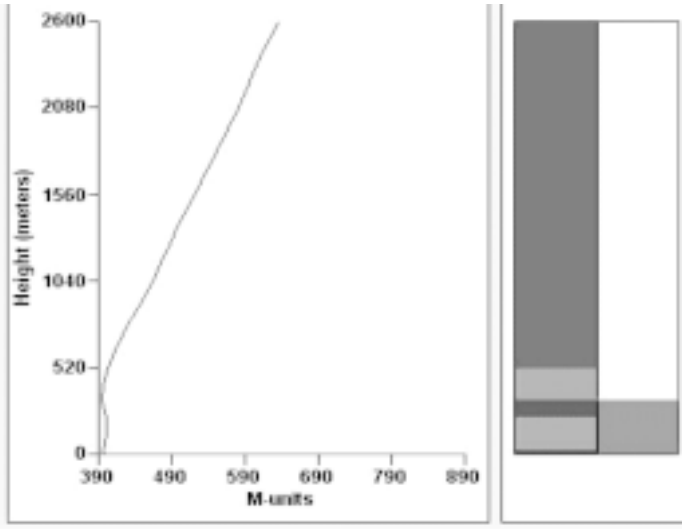

Figure 7. Refractivity in AREPS, blue is normal, green is super-refraction and pink is trap.

propagation in AREPS, all elevation radar waves can pass through terrain around the RCWF under standard atmospheric conditions (Fig. 8a). Fig. 8b shows the simulated vertical profile from Fig. 6. Some of the waves were blocked by terrain, and some low elevation angle waves reached the sea at 100 km from the radar station. Atmospheric refractivity can be simulated in WRF and the results account for the abnormal propagation of this case.

Although AREPS simulates all direction traces in a single profile, atmospheric conditions vary. Therefore, more vertical profiles could be applied in the GIS with WRF output. According to AREPS ray trace theory, supposing that the range of a horizontal transition radar wave is 1 km, the height and elevation angle variation change can be calculated and spatial coordinates assigned. In Fig. 2, range r' is $1\,\mathrm{km}\times\cos(\alpha)$, elevation angle $\alpha \neq 0$, and $\alpha' = \alpha + r' \times dMdh_j$, $h' = h + (\alpha'^2 - \alpha^2)/0.002\ dMdh_j$.

This study focuses on the position of northwestern

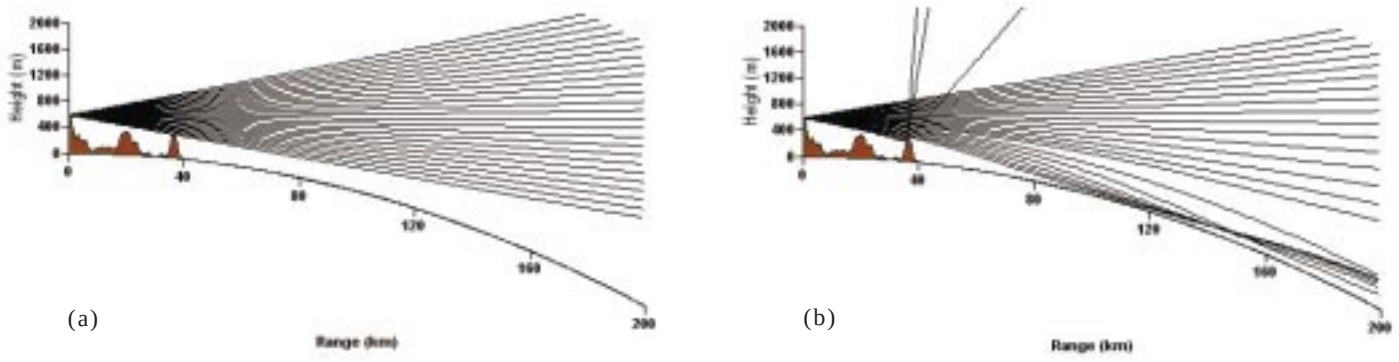

Figure 8. Ray trace calculated with single vertical profile by AREPS, (a) standard atmosphere, (b) with refractivity, the horizontal axis for distance (km), and vertical axis for height (m).

radar waves from the station to the sea's surface and only the directions of azimuth at 200–10° (clockwise) are simulated. The interval of each ray is 5°. Considering terrain interference, the radar beam reached the sea's surface and at a height lower than that of the terrain before it stopped transiting. Terrain height is set by WRF; the height of the radar is 15 m above the ground. The ray traces adapt to the WRF grid and are integrated every 1 km from the radar station to a distance of 230 km. During integration, the GIS picks terrain height and vertical profile of a corresponding point while ray height is used to obtain the *dMdh*. Furthermore, duct intensity is weak when using the meteorological model output. Consequently, duct intensity is strengthened.

In the GIS simulation, *dMdH* was a key factor in propagation, and the *dMdH* around the radar station was adjusted so as to lower the height of the ray and allow the radar wave to enter the trapping layer over the sea. If a wave was blocked by terrain, reached the sea's surface or reached a maximum distance (230 km in this study), azimuth ray trace simulation stops. The research flow is shown in Fig. 1 while Fig. 9 shows the simulation results.

Based on the simulation that took place at 18 UTC on July 3rd, Fig. 9a shows a ray with a 0.5° elevation angle that was blocked by the southern mountain range. Rays in the azimuth at 200–235° cannot pass through the terrain, whereas those between 265–10° reached the trapping layer, and the height of rays decreased. In Fig. 9b, a ray with a 1.5° elevation angle was blocked at directions of 205°, 215° and 200° while rays in other directions reached the sea. The angle in the azimuth of 255–10° was trapped, the height of rays decreased to the sea's surface, and the rays were deflected 10° to the south. Consequently, the echo at a 1.5° elevation angle was deflected south. For these two elevation angles, rays at 200–255° azimuths were both affected by mountains and did not reach the sea. In a 3D view (Fig. 9c), the height of the ray decreased after reaching the sea. Thus, the GIS and display the relationship between ray trace and echo location and is able to determine that the echo is an anomaly.

Using the same settings to analyze the simulation at 00 UTC on July 4th (Fig. 9d), a 0.5° elevation angle, with rays in an azimuth of 200–255°, were blocked by the southern mountain range. Those in an azimuth of 290–310° were also blocked and thus did not reach the sea. Therefore, refraction at this point is more apparent than it was at 18 UTC on July 3rd, according to the actual observations. When simulating a 1.5° elevation angle (Fig. 9e), the effects of terrain interference decreased. All rays in the south passed through the terrain, and only rays in the 200–310° azimuth were affected. Furthermore, an echo was not evident. The ray extended over the sea close to the location at 18 UTC on July 3rd. The duct intensity requires additional adjustment and testing. Figure 9f is a 3-D display of the simulation at 00 UTC on July 4th.

The simulations of Atkinson *et al*[9] and Haack *et al*[11] both indicated that duct intensity was too weak and duct height was too low. In this study, radar height was not changed to assess terrain interference; only duct intensity was adjusted. Inferred from the ray trace, the real altitude of RCWF is 740 m, and rays with elevation angles of 0.5° and 1.5° bend downward toward the sea at roughly 120 km from RCWF. The *dMdH* is stronger than -250 M Km^{-1} on average from Eqn. (3) and it could not be observed by current instruments. Rays propagate from different distances on land to the sea. Thus, the program developed in this study takes WRF simulation results as a reference. The intensity of ducts is apparent within 25 km of the radar station. Duct intensity was enhanced so that ray height was not excessively high when entering the duct layer over the sea.

A trapping layer over the sea suggests that rays can reach the sea's surface. Thus, duct intensity over the sea should be adapted. When ray angle remains positive, if $dMdH < 0$, ray height should be lowered to enhance duct intensity. Radar propagation is affected by complex atmospheric and terrain conditions. However, as the weather model simulates all physical processes, more accurate results may require additional research. Simulation of a ray trace and adjustment of *dMdH* in this study provides a useful reference for boundary parameters adjustment and needs further research.

5. DISCUSSION

Along with progress in war science and technology, battlefield commanders not only need to consider how

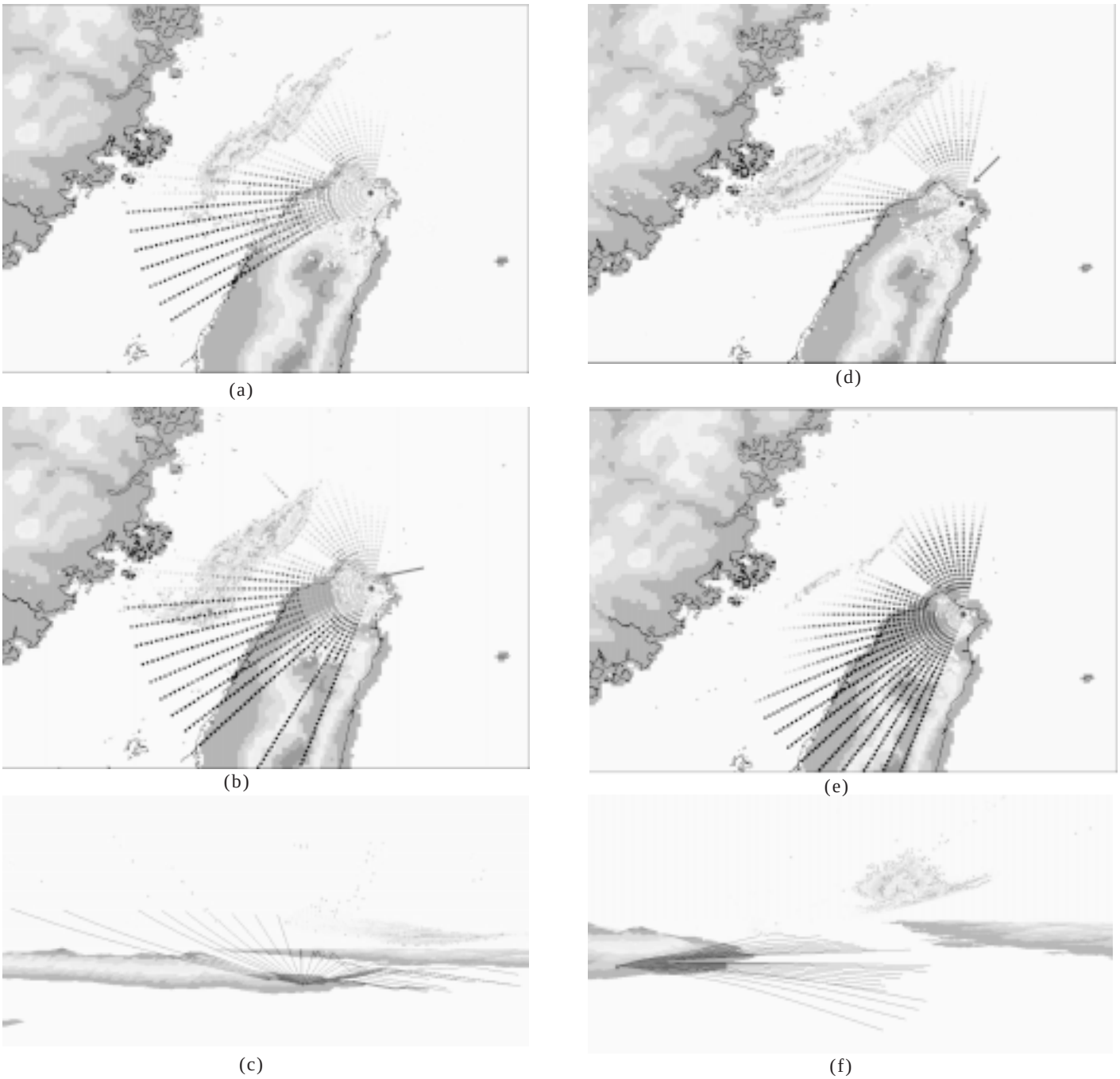

Figure 9. Ray trace simulation and radar reflectivity in GIS, (a), (b), stand for 0.5°, 1.5° elevation angle 2-D and (c) for 3-D view respectively of July 3, 18 UTC. (d), (e), (f) stand for July 4, 00 UTC. In 2-D view, red dots indicate the ray trace, deeper color stands for higher altitude, the dot distance is 5 km. In 3-D view, blue lines for 1.5° elevation, red lines for 0.5°. The 0.5° elevation radar reflectivity is shown. The view point is at northeast of radar station, vertical exaggeration is about 100 to enhance the visual effect.

meteorological conditions influence military action as well as weaponry. Thus, the demand for meteorological intelligence is high. Accurate, timely and reliable meteorological intelligence may provide commanders with the essential information they need to gain the upper hand on the battlefield. This research mainly aims to validate the feasibility of developing a Common Operational Picture in the GIS. It uses the GIS to forecast abnormal radar propagation.

This study examines an anomaly echo case in the northern Taiwan Straight, as observed by the RCWF station on the night of July 3, 2003. Radar observation and WRF outputs are integrated in the GIS, and applications of meteorological data are presented. Atmospheric refraction computation and ray trace simulation was conducted using AREPS and the GIS.

Through this case study, a ray trace simulation was carried out using the GIS with the numerical weather model to determine the position of abnormal radar reflectivity. Extending the application to simulate the environment according to the requirements of users, such as input radar sites or

radar frequencies, model output can be tailored to customer-oriented decision-making supports. Field commanders can better understand weather conditions which in turn can help them optimally deploy electromagnetic equipment. This serves as the foundation of a COP.

Although this study on the simulation of atmospheric refraction and terrain interference was successful, further studies focusing on factors such as the effects of liquid particles on propagation loss, diffraction, and tropospheric scattering, need to be conducted in order to develop a more extensive radar propagation system (Haynes, *et al.*[35]).

Furthermore, terrain height between systems differ, producing variable ray trace results. Take the RCWF station as an example. Its height is approximately 740 m. However, in the WRF 5 km grid, the corresponding height is only 288 m. The height of digital terrain elevation data level 0 (DTED0) in AREPS is 560 m. This difference presents a significant challenge for meteorological model simulation. The integration and application of terrain data in different systems warrants further research.

6. ACKNOWLEDGEMENTS

The authors would like to thank the Central Weather Bureau for RCWF radar data and National Center of Atmospheric Research for its free WRF model. In addition, many thanks to funding support under National Science Council under Contract No. NSC 93-2623-7-014-023, NSC 94-2623-7-232-001, NSC 95-2623-7-014-016, NSC 95-2623-7-232 -001–D which made this work possible.

REFERENCES

1. Kuo, Ying-Hua & Chen, George Tai-Jen. The Taiwan area mesoscale experiment (TAMEX): An overview. *Bull. Ameri. Meteor. Soc.*, 1990, **71**(4), 488-503.
2. Lin, Yuh-Lang. Orographic effects on airflow and mesoscale weather systems over Taiwan. *TAO*, 1993, **4**(4), 381-420.
3. Chen, George Tai-Jen & Chou, H. C. General characteristics of squall lines observed in TAMEX. *Monthly Weather Rev.*, 1993, **121**, 726-33.
4. Chien-Yuan, Chen; Lin, Lee-Yao; Yu, Fan-Chieh; Lee, Ching-Sheng; Tseng, Chun-Chieh; Wang, An-Hsiang & Cheung, Kei-Wai. Improving debris flow monitoring in Taiwan by using high-resolution rainfall products from QPESUMS. *Nat. Hazards*, 2007, **40**(2), 447-61.
5. Vasiloff, V. Steven; Seo, Dong-Jun; Howard, W. Kenneth; Zhang, Jian; Kitzmiller, H. David; Mullusky, G. Mary; Krajewski, F. Witold; Brandes A. Edward; Rabin, M. Robert; Berkowitz S. Daniel; Brooks, E. Harlod; McGinley, A. John; Kuligowski, J. Robert & Brown,G. Barbara. Improving QPE and very short term QPF. *BAMS*, 2007, 1899-1911.
6. Moszkowicz, S.; Ciach, G.J. & Krajewski, W.F. Statistical detection of anomalous propagation in radar reflectivity patterns, *J. Atmos. Oceanic Technol.*, 1994, **11**, 1026-34.
7. Borsum, D.L. Doppler dilemma delineates danger from dirt. National weather service western region tech. attachment, 95-07, 1995, 7pp.
8. Lu, F.C. & Chu, Y.H. Experiment of evaporation ducting in Taiwan Area(II). Research Report, NSC 94-2623-7-232-001, 2004, pp. 90.
9. Atkinson, B.W.; Li, J.G. & Plant, R.S. Numerical modeling of the propagation environment in the atmospheric boundary layer over the Persian Gulf. *J. App. Meteor.*, 2001, **40**, 586-603.
10. Zhu, M. & Atkinson, B.W. Simulated climatology of atmospheric ducts over the Persian Gulf. *Boundary-Layer Meteor.*, 2005, **115**, 433-52.
11. Haack, T. & Burk, S.D. Summertime marine refractivity conditions along coastal California. *J. Appl. Meteor.* 2001, **40**, 673-687.
12. Habermann T. What is GIS (for Unidata)? *Bull. Ameri. Meteor. Soc.* 2005, **86**, 174-75.
13. Ramamurthy, M. Unidata's blueprint for 2008. *Bull. Ameri. Meteor. Soc.* 2005, **86**, 179-80.
14. Shipley T.S. GIS applications in meteorology or adventures in a parallel universe. *Bull. Ameri. Meteor. Soc.*, 2005, **86**, 171-73.
15. Kucera, P.A.; Krajewski, W.F. & Toung, C.B. Radar beam occultation studies using GIS and DEM technology: An example study of Guam. *J. Atmos. and Ocean Tech.*, 2004, **21**, 995-1006.
16. Krajewski, W.F.; Ntelekos, A.A. & Goska, R. A GIS-based methodology for the assessment of weather radar beam blockage in mountainous regions: Two examples from the US NEXRAD network. *Computers & Geosciences*, 2006, **32**, 283-302.
17. Xie, H.J.; Zhou, X.B.; Vivoni, E.R., Hendrickx M.H. & Small, E.E. GIS-based NEXRAD Stage III precipitation database: Automated approaches for data processing and visualization. *Computers & Geosciences*, 2005, **31**, 65-76.
18. Keuhlen, D.T.; Bryant, O.L. & Young, K.K. The common operational picture in Joint Vision 2020: A less layered cake, joint forces staff college, joint and combined warfare school, 2002, 30 p. www.jfsc.ndu.edu/current_students/documents_policies/documents/jca_cca_awsp/common.doc.
19. Richmond, P.W.; Blais C.L. & Goerger, N.C. Development of a ground vehicle maneuver ontology to support the common operational picture, cross talk. *J. Def. Soft. Engg.*, 2006, **19**(7), 26-30.
20. Debye, P., Polar molecules. Dover Publications Inc., New York, 1929, pp. 172.
21. Bean, B.R. & Dutton, E.J. Radio Meteorology. Dover Publications, 1968, pp. 435.
22. Babin, S.M. Surface duct height distributions for Wallops Island, 1985-1994. *J. Appl. Meteor.*, 1996, **35**, 86-93.
23. Babin, S.M.; Young, G.S., & Carton, J.A. A new model for the oceanic evaporation duct. *J. Appl. Meteor.* 1997, **36**, 193-204.
24. Rinehart, E.R. Radar for meteorologists, Third Edition. Rinehart Publications, 1997, pp. 418.
25. Patterson, W.L.; Hattan,C.P.; Lindem, G.E.R.; Paulus,

A.; Hitney, H.V.; Anderson, K.D. & Barrios, A.E. Engineer's refractive effects prediction system (EREPS), Technical Document 2648, 1994. pp. 179.

26. Gabella, M. & Perona, G. Simulation of the orographic influence on weather radar using a geometric-optics approach. *J. Atmos. and Ocean. Tech.*, 1998, **15**(6), 1485-94.
27. Siddiqui, M.N.; Jamil, Z. & Afsar, J. Monitoring changes in riverine forests of Sindh-Pakistan using remote sensing and GIS techniques. *Advances in Space Research*, 2004, **33**, 333-37.
28. Ng, S.P.; Dimitroulopoulou, C.; Grossinho, A.; Chen, L.C. & Kendall M. $PM_{2.5}$ exposure assessment of the population in lower Manhattan area of New York City after the World Trade Center disaster. *Atmospheric Environment*, 2005, **39**, 1979-92.
29. Wilhelmi V.O & Betancourt, L. Terri. Evolution of NCAR's GIS initiative: Demonstration of GIS interoperability. *Bull. of the Ameri. Meteor. Soc.*, 2005, **86**, 176-78.
30. Wilhelmi V.O. & Brunskill, J.C. Geographic Information Systems in weather, climate and impacts. *Bull. of the Ameri. Meteor. Soc.*, 2003, **84**, 1409-14.
31. Yuan M. Beyond mapping in GIS applications to environmental analysis. *Bull. of the Ameri. Meteor. Soc.*, 2005, **86**, 169-70.
32. Chu, Chang-Min; Chen, C.N.; Lu, F.C. & Wang, J.L. Case study of abnormal radar echoes in the northern Taiwan Strait on July 3rd, 2003 Part I: Environment analysis, Atmospheric Sciences. *Meteor. Soc. of Republic of China*, 2007, **35**, 219-40.
33. Skamarock, W.C.; Klemp, J.B.; Dudhia, J.; Gill, D.O., Barker, D.M.; Wang, W. & Power, J.G. A description of the advanced research WRF version 2. NCAR/TN-468+STR, National Center for Atmospheric Research, technical note, 2005, pp. 88.
34. Chu, Chang-Min; Chen, C.N.; Lu, F.C. & Wang, J.L. Case study of abnormal radar echoes in the northern Taiwan Strait on July 3rd, 2003 part II: Numerical simulation, Atmospheric Sciences. *Meteor. Soc. of Republic of China*, 2007, **35**, 241-60.
35. Haynes, J.M.; Marchand, R.T.; Luo, A.; Bodas-Salcedo, A. & Stephens, G.L. A multipurpose radar simulation package: Quick beam. *Bull. Ameri. Meteor. Soc.*, 2007, **88**, 1723-23.